Solar wind electron distribution functions inside magnetic clouds

Teresa Nieves-Chinchilla[1] and Adolfo F. Viñas[1]

[1]   This paper presents a study of the kinetic properties of the electron velocity distribution functions within interplanetary magnetic clouds, since they are the dominant thermal component and can contribute as much as 50% of the total electron pressure within the clouds. The study is based on high time resolution data from the Goddard Space Flight Center Wind Solar Wind Experiment vector electron and ion spectrometer. Studies on interplanetary magnetic clouds have shown observational evidence of anticorrelation between the total electron density and temperature, which suggests a polytrope law $P_e = \alpha n_e^\gamma$ for electrons with the constant $\gamma \approx 0.5 < 1$. This anticorrelation and small γ values are interpreted in the context of the presence of highly non-Maxwellian electron distributions (i.e., nonthermal tails) within magnetic clouds. We have revisited some of the magnetic cloud events previously studied to quantify the nature of the nonthermal electrons by modeling the electron velocity distribution function using Maxwellian and kappa-like distribution functions to characterize the kinetic nonthermal effects. The results show that the electron density-temperature anticorrelation is not a unique feature of magnetic clouds. Within magnetic clouds, κ values are generally small, in the range of 1.6–5.4; however, such small values are also typical of regions outside the clouds. We have shown that the density-temperature anticorrelation of the electron moments is persistently consistent with similar density-temperature anticorrelation in the electron halo component of the velocity distribution function and essentially little or no correlation was obtained for the core component. This result clearly shows that the temperature and density of the suprathermal components play a significant role in the temperature-density anticorrelation because of a relative enhancement of the halo component abundance to the total density.

Citation: Nieves-Chinchilla, T., and A. F. Viñas (2008), Solar wind electron distribution functions inside magnetic clouds, *J. Geophys. Res.*, *113*, A02105, doi:10.1029/2007JA012703.

1.   Introduction

[2]   Magnetic clouds (MC) were first investigated by *Burlaga et al.* [1981] and were characterized by a minimum of three basic physical properties: (1) an increase in the magnitude of the magnetic field, (2) a large smooth rotation of the magnetic field vector, and (3) a low proton thermal temperature within the magnetic cloud. Other researchers have implicitly suggested that magnetic clouds are also characterized by an observed anticorrelation between the electron density and the electron temperature inside the structures (*Osherovich et al.* [1993, 1998], *Hammond et al.* [1996], *Sittler and Burlaga* [1998], *Gosling* [1999], and *Skoug et al.* [2000a, 2000b] among many others). The interpretation of such anticorrelation is still unclear and has been a topic of intense debate among many researchers. One interpretation of this anticorrelation [e.g., *Hammond et al.*, 1996; *Gosling*, 1999; *Skoug et al.*, 2000a, 2000b] is that it is a consequence of the tendency to achieve local total pressure balance as it evolves out from the Sun and

therefore the so called "polytrope index" corresponding to the slope of the electron temperature-density anticorrelation provides no information about the thermodynamic state of the cloud. An alternative interpretation by other authors [e.g., *Osherovich et al.*, 1993, 1998; *Sittler and Burlaga*, 1998] suggested that such anticorrelation provides evidence about the thermodynamics "polytrope relation" $P_e = \alpha n_e^\gamma$ of magnetic clouds, since the electron thermal energy dominates the proton thermal energy within the cloud and the resultant value for the "polytrope" index $\gamma < 1$ controls the temperature evolution of the magnetic cloud. *Sittler and Burlaga* [1998] suggested that high moment temperatures are associated with the halo component, which is anticorrelated with the total density without requiring an anticorrelation between the core electron temperature and density. Furthermore, *Fainberg et al.* [1996] and *Osherovich et al.* [1998] argue that $\gamma < 1$ indicates the presence of nonthermal plasmas, which is not inconsistent with kinetic physics and that the proportionality constant α is a functional of the entropy S. According to *Fainberg et al.* [1996], nonthermal electrons can contribute as much as 50% of the total electron pressure within magnetic clouds and the electrons are highly non-Maxwellian. This result is again supported by the study carried out by *Sittler and Burlaga* [1998] using Voyager electron data. *Dasso et al.* [2001] has also shown

---

[1]Geospace Physics Laboratory, NASA Goddard Space Flight Center, Greenbelt, Maryland, USA.
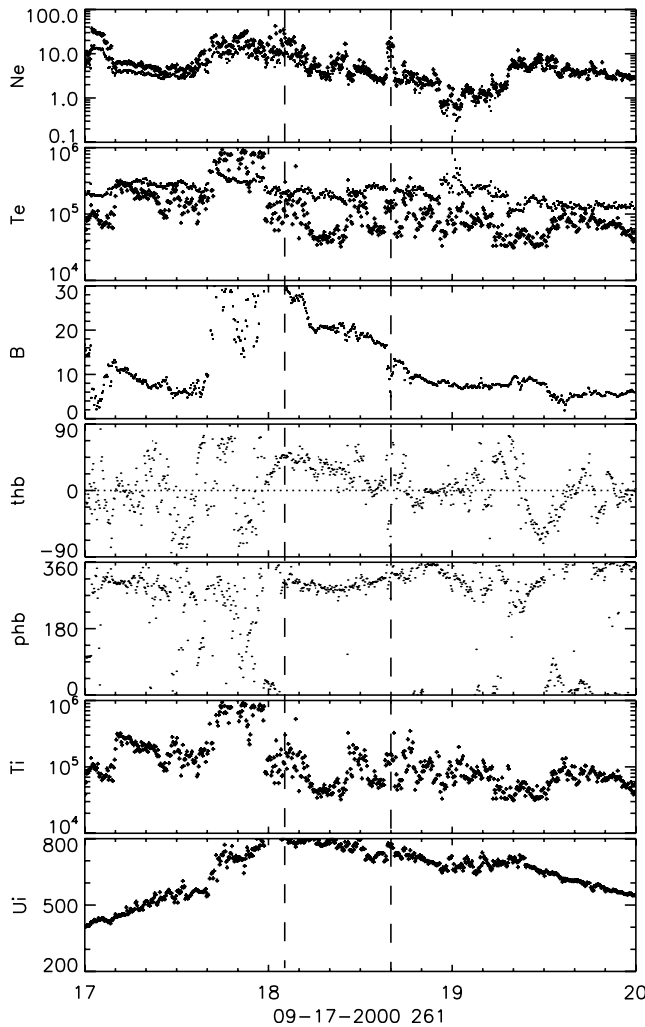
Figure 1. Plots of plasma and magnetic field data for the magnetic cloud event of 17 September 2000, showing from top to bottom the electron density N_e (#/cm3), temperature T_e (°K), the magnitude of the magnetic field $|B|$ (nT), the elevation and azimuth angles of the B field and the proton plasma temperature T_p (°K), and bulk speed U_p (km/sec). The vertical lines represent the intervals for the magnetic cloud.

that the condition $T_e \gg T_p$ and that the electron are anisotropic with $T_{e\perp}/T_{e\parallel} < 1$ are clearly sustained for more than 85% of the time duration of all the magnetic clouds they have investigated. They have also shown that such conditions influence the excitation of electromagnetic ion-cyclotron waves inside interplanetary coronal mass ejections and magnetic clouds [e.g., *Dasso et al.*, 2003].

[3] The purpose of this work is to investigate the global nature of the electron velocity distribution functions (VDF) inside and outside magnetic clouds in order to ascertain the nature of the nonthermal distributions and shed some light onto this controversial issue of the anticorrelation. The procedure we follow is to model the nonthermal distribution effects by a Tsallis kappa-like (i.e., power of $-\kappa$) distribution, which has been obtained from nonextensive statistical mechanics [*Tsallis*, 1988; *Tsallis and Brigatti*, 2004]. If

nonthermal tail effects are the source for the anticorrelation between the moment electron temperature and density and if the kappa-like distribution is a reasonable representative model of nonthermal effects, then the electron velocity distribution within magnetic clouds should show indication for small κ values when $\gamma < 1$. We have reviewed three typical magnetic clouds observed by the Wind Solar Wind Experiment (SWE) vector electron and ion spectrometer (VEIS) (see Figures 1, 2, and 3) that have been previously investigated by other authors in order to examine the structure of the electron VDFs since the temperature-density anticorrelation and the resultant index $\gamma < 1$ has been linked to the existence of non-Maxwellian VDFs.

[4] Previous studies of solar wind electrons have used the conventional (i.e., power of $-(\kappa + 1)$) kappa distribution [*Olbert*, 1968; *Vasyliunas*, 1968] to model kinetic properties of electrons, such as suprathermal tails and heat flux (*Maksimovic et al.* [1997] and *Dorelli and Scudder* [1999] among others). These studies have been successful in describing nonthermal features of the electron velocity distribution such as anisotropy, bidirectional heat flux, and core-halo-strahl-distributions in the fast solar wind (see also *Feldman et al.* [1975] and the review by *Marsch* [2005]). The conditions in the solar corona from which the solar wind emanates together with the global structure of the magnetic and electric fields are responsible for the shapes of the electron velocity distribution functions in the interplanetary media. Among these features, i.e., the bidirectional heat flux events, are potentially valuable measurements that can provide information about the large-scale topological structure of the magnetic field within magnetic clouds and/or other coronal mass ejection types [*Gosling et al.*, 1987; *Pilipp et al.*, 1987].

[5] The paper is organized as follows: section 2 presents a brief discussion of the electron plasma moment and magnetic field data used in our study. It also shows the magnetic cloud events selected for the study and the temperature-density anticorrelation for each event. In section 3 we discuss the theoretical model and the analysis used to investigate the electron velocity distribution functions. Section 4 shows a summary of our results. In section 5 we present theoretical ideas and their implications that show a connection between the polytrope relation and the kappa-like distribution. In section 5 we conclude with a summary and discussion of our results.

2. Wind SWE VEIS Electron Moment Data

[6] The electron moment calculations and the three-dimensional (3-D) VDF measurements used in our study have been obtained from the 3 s time resolution data of the Wind SWE VEIS (details of the instrument characteristics are given by *Ogilvie et al.* [1995] (see Figure 1). The VEIS consists of six programmable analyzers which forms three pairs of mutually orthogonal sensors. The analyzers measure electrons in the energy range from 7 eV to 25 keV in 16 energy steps with an energy resolution of about 6%. However, for solar wind electron studies the effective energy range has been set from 10 eV to 3 keV. Each sensor full energy sweep takes 0.5 s, which implies that the highest time resolution moment is determined in 0.5 s, but for statistical purposes the moments have been averaged out
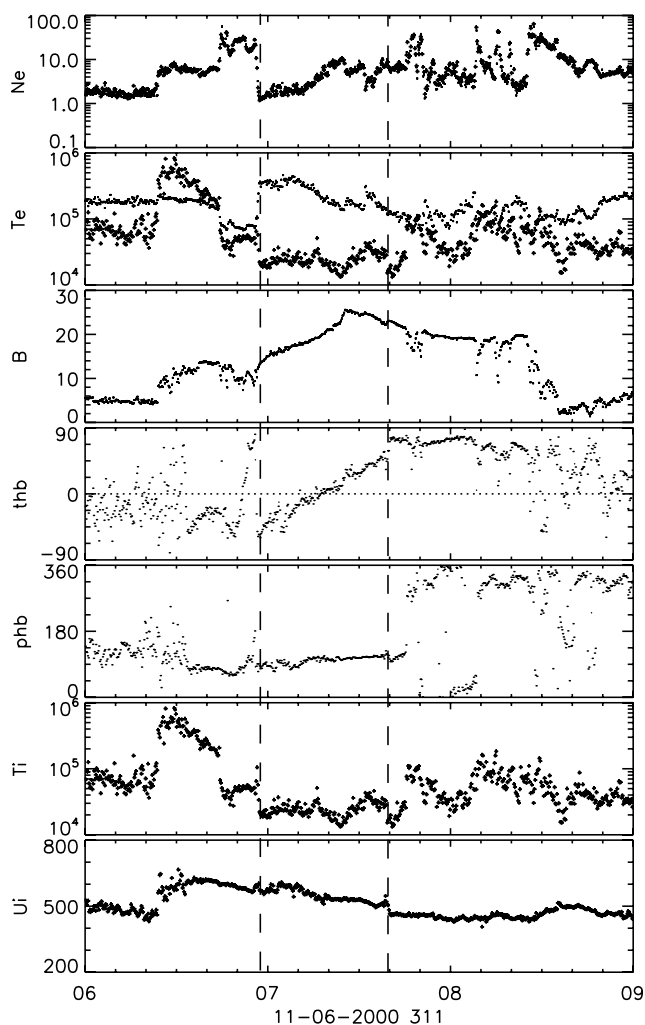
Figure 2. Same as Figure 1 but for the magnetic cloud event of 6 November 2000.

tively. The bottom plot also has the magnitude of the solar wind proton bulk velocity. The magnetic cloud interval has been identified by the vertical dashed lines and in accordance with *Burlaga et al.*'s [1981] cloud criterion. Table 1 shows a summary of the time intervals selected for each magnetic cloud studied in this paper. The cloud boundaries are in agreement with other authors and we have also pointed out any other additional structure (e.g., magnetic flux rope) within the cloud as indicated by *Russell and Shinde* [2005], *Nieves-Chinchilla et al.* [2005], and *Lepping et al.* [2006]. These clouds were selected because they showed a clear electron temperature-density anticorrelation which is also verified by the 3DP Berkeley electron observations.

[8] The scatterplots in Figure 4 show the total moment temperature versus total moment density inside the magnetic cloud for the events of interest using the Wind SWE VEIS measurements. For comparison purpose we also show similar plots from the 3DP Berkeley data. Both instruments show consistent temperature-density anticorrelation. The figures also show the Wind SWE VEIS data together with
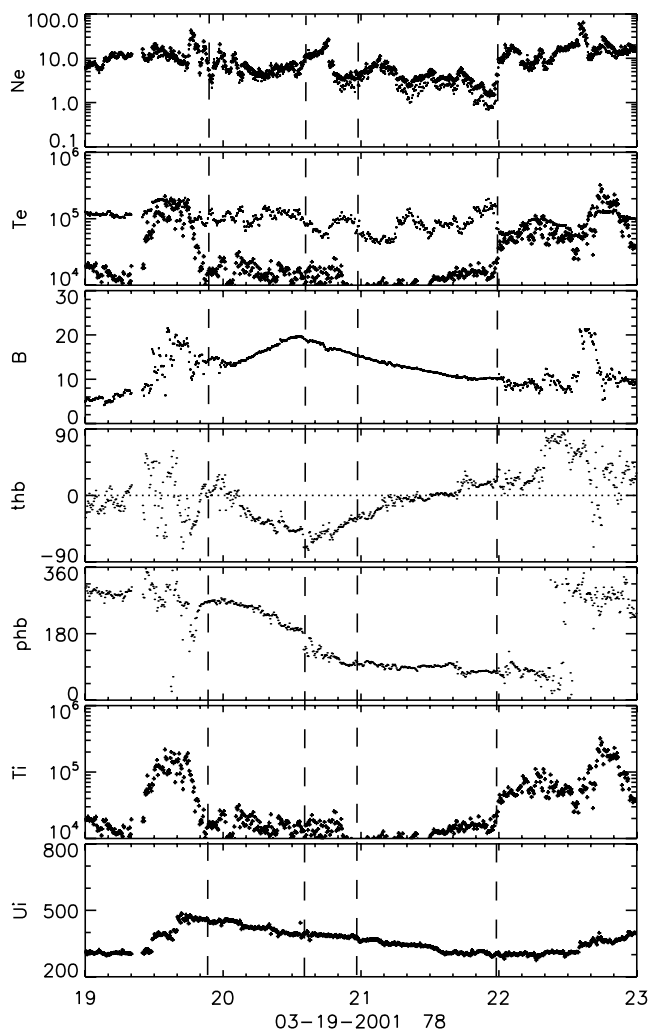
to the full satellite spin period of 3 s. The moment calculations has been corrected by the spacecraft potential (which usually ranges between 3–15 V depending upon solar conditions) using either the proton and alpha measurements from the Wind SWE Massachusetts Institute of Technology (MIT) Faraday cup or the electron density estimates of the plasma frequency line from the WIND/WAVES experiment. The higher-order moments (e.g., pressure and heat flux) have been calculated by properly shifting the VDFs into the solar wind frame using the proton bulk velocity interpolated to the electron times. The moment results presented here have been compared with similar calculations from the Berkeley 3DP Plasma Analyzer instrument [*Lin et al.*, 1995] aboard the same spacecraft and both data sets show a clear temperature-density anticorrelation.

[7] Figures 1–3 show the electron and proton moment bulk plasma data and magnetic field components for the three magnetic cloud events observed by the Wind spacecraft during an excursion into the solar wind, which occurred on 18 September 2000, 6 November 2000, and 19 March 2001. The electron and proton densities and temperatures are identified by the dots and crosses respec-

Figure 3. Same as Figure 1 but for the magnetic cloud event of 19 March 2001.

Table 1. Time Intervals of the Events Studied in This Article, Satisfying *Burlaga et al.*'s [1981] Plasma and Magnetic Field Criteria for MCs[a]

	Start Interval		End Interval	
	Date of Year	Hour	Date of Year	Hour
18 September 2000	262	2	262	16
Front interval	261	0	261	23
Rear interval	262	16.5	263	0
6 November 2000	311	23	312	16
Front interval	310	0	311	20
Rear interval	312	18	312	24
19 March 2001 ST1	78	21	79	14
19 March 2001 ST2	79	23.5	80	23.8
Front interval	77	0	77	5.4
Rear interval	81	1.5	81	23

[a]These intervals also showed a clear electron density-temperature anticorrelation. Also included are the time intervals of the front and rear regions selected for data analysis outside the magnetic clouds for each event.

50 points bin-averaged values and a weighted least squares line fit $\ln T_e = (\gamma_e - 1)\ln n_e + C$ of the anticorrelation. The results of this linear fit shows that the slope of the linear correlation (i.e., $\gamma_e - 1$) ranges from 0.2 to 0.5 for the three events, as illustrated in Figure 4. Similar trends are observed in the 3DP Berkeley data. The magnetic cloud event of 19 March 2001 seems to have a second structure which has been previously identified as a flux tube by *Nieves-Chinchilla et al.* [2005], *Russell and Shinde* [2005], and V. A. Osherovich (private communication, 2005) and they are identified as ST1 and ST2 in the plots.

[9] Figure 5 shows similar scatterplots of the temperature-density anticorrelation as in Figure 4 but outside (in front and rear) of the magnetic cloud events using the Wind SWE VEIS data. The time interval boundaries for the front and rear data intervals used for analysis in this paper are also summarized in Table 1. Note that of the three events in this study, two show (i.e., 18 September 2000 and 6 November 2000) a clear temperature-density anticorrelation outside (in front) the magnetic cloud, whereas one event shows basically little or no correlation. This implies that such anticorrelation is not unique to the interior of the magnetic clouds and they can also be observed outside as also noticed by *Skoug et al.* [2000a]. The intervals chosen for the front and rear regions of the MCs were carefully selected so that *Burlaga et al.*'s [1981] plasma and magnetic field conditions, which define a magnetic cloud, are not met. Furthermore, these intervals were selected in the ambient solar wind, well away from any shock or sheath associated with the magnetic clouds.

3. Modeling and Analysis of the Electron Velocity Distribution Function

[10] In this section we investigate the nature of the suprathermal VDF by examining and modeling the global structure of the electron velocity distribution function inside and outside magnetic clouds. The VDF data sets used in this study are the reduced $F(v_\parallel)$ distribution functions obtained by folding the original 3-D distributions into the $(v_\parallel, v_\perp)$ space (e.g., assuming the gyrotropy condition) using the

measured 3 s magnetic field averages and then integrating the 2-D distributions in the $v_\perp$ space to yield a 1-D distribution function representative of the direction along the magnetic field. The reasons for using the reduced distribution function are (1) the observed temperature-density anticorrelation appears to be similar in the full moment as well as in the moments of the reduced distributions, (2) that we expect suprathermal tails to form easily along the parallel direction because of the electrons free mobility along the magnetic field lines, and (3) they provide an easier visual display of the quality of the fits.

[11] We studied the VDFs using two different models. Both models use a kappa-like distribution function that was obtained from nonextensive statistical mechanics formalism by *Tsallis* [1988] and applied to the context of space physics by *Leubner* [2004a, 2004b]. Throughout this paper we will use only the 1-D and 3-D forms of the nonextensive Tsallis kappa-like distribution and not the conventional form. An important difference between the conventional kappa distribution [*Olbert*, 1968; *Vasyliunas*, 1968] and the Tsallis kappa-like distribution is that the later has a more pronounced tails as compared to the conventional form. Also, the normalization and the temperature (second moment) are different from the conventional kappa distribution. More details about the differences between the conventional kappa distribution and the Tsallis kappa-like distribution are clearly discussed by *Leubner* [2004a], and we will not dwell further on the characteristics of these two forms. In the first model we represented the full 1-D reduced distribution in terms of a (single) kappa-like distribution given by

$$f_\kappa(v) = \frac{n}{\pi^{1/2}w} \frac{\Gamma(\kappa)}{\kappa^{1/2}\Gamma(\kappa - 1/2)} \left[1 + \frac{(v - \delta U)^2}{\kappa w^2}\right]^{-\kappa}, \quad (1)$$

where n is the electron density, $w = \sqrt{2\kappa_B T/m}$ is the electron thermal velocity that is related to a Maxwellian temperature T, m is the electron mass, κ_B is the Boltzmann constant, δU is a parallel electron drift velocity correction, and Γ is the gamma function. The definition of temperature is a concept applied to systems in thermal equilibrium, but the effective thermal velocity and temperature of a kappa-like distribution (nonthermal) is obtained from the second moment of the distribution function which gives a relationship between the effective temperature T_{eff} in terms of the energy density for a one-dimensional case as

$$T_{eff} = \frac{1}{n} \int (mv^2) f_\kappa(v) dv \quad (2)$$

and reduces to $T_{eff} = (\kappa/(\kappa - 1/2)) mw^2/2$, where $T_{eff} = (\kappa/(\kappa - 1/2))T$. This clearly shows that for finite κ values the effective temperature of a kappa-like distribution is greater than a Maxwellian temperature and in the limit as κ approaches infinity the effective kappa-like distribution temperature T_{eff} approaches the Maxwellian temperature T. Because the observed VDFs have been already shifted into the proper solar wind frame using the proton velocity from the MIT Faraday's cup instrument, we have included a small electron velocity correction to account for any differences between the proton and electron bulk velocities.
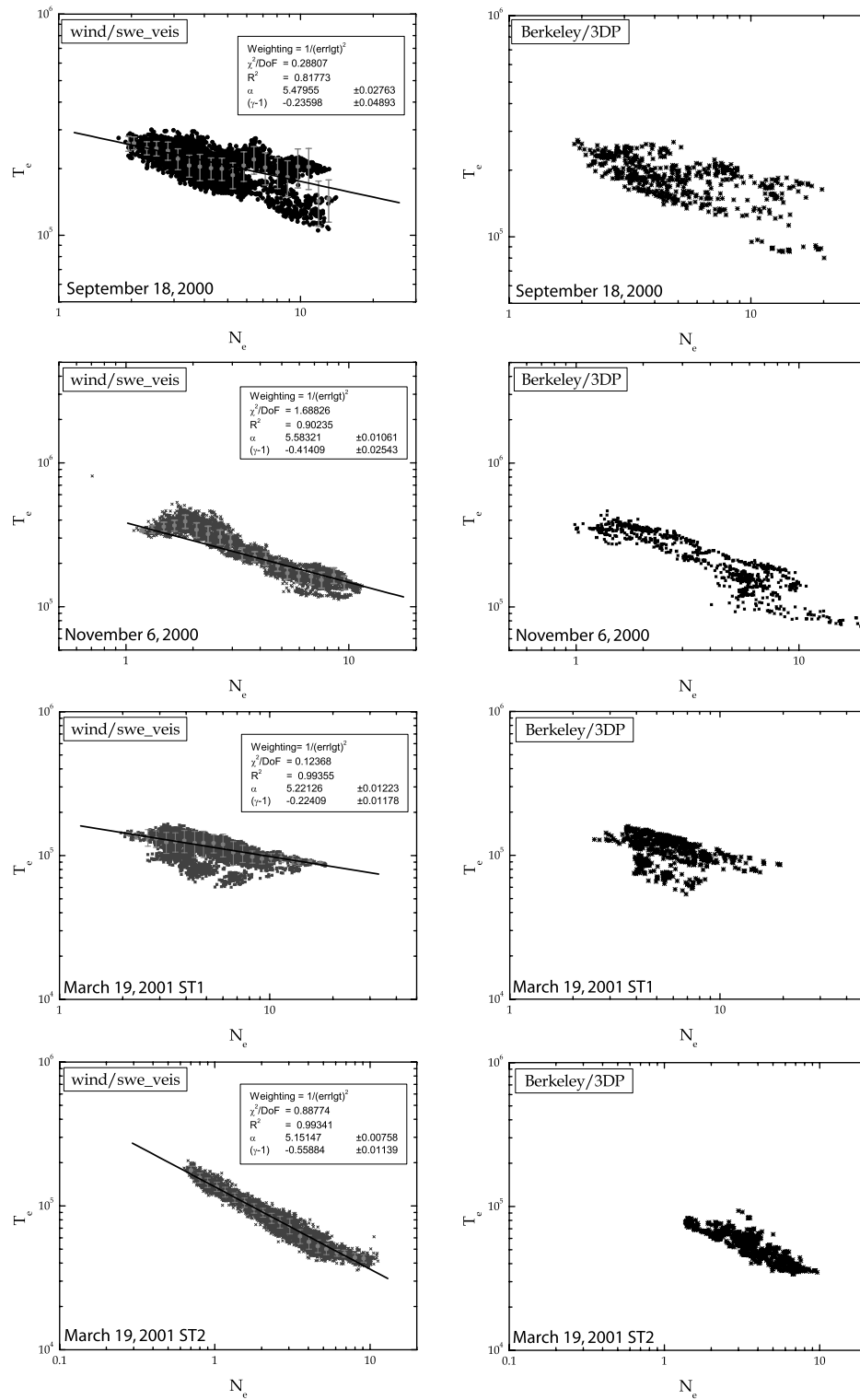
Figure 4. Scatterplot of the electron moment temperature and moment density inside the three magnetic cloud events as measured by the Wind VEIS and 3DP Berkeley electron analyzers. The plots also show a fitting analysis for the Wind VEIS data.
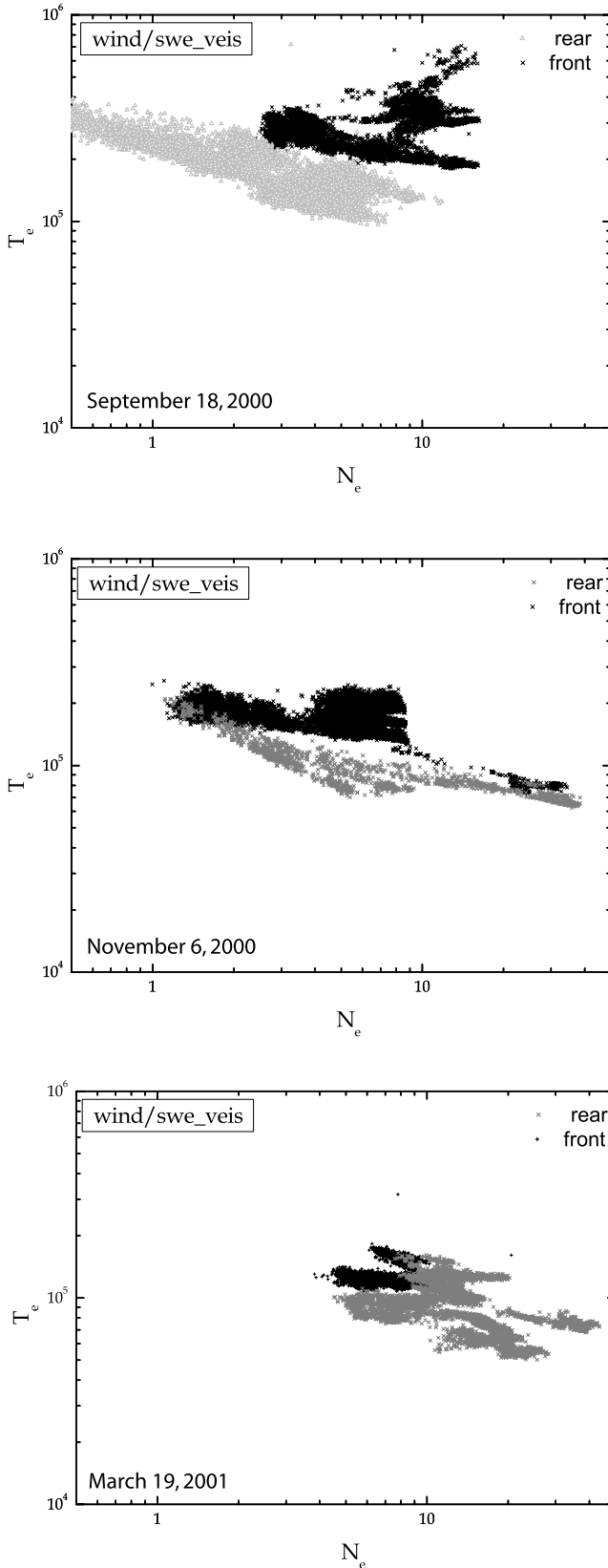
Figure 5. Scatterplot of the electron moment temperature and moment density outside (front/rear) the three magnetic cloud events as measured by the Wind VEIS analyzer.

[12] The second model uses a superposition of a core Maxwellian and a halo kappa-like distribution (i.e., $f = f_c^M + f_h^\kappa$) where the core distribution is given by

$$f_c^M(v) = \frac{n_c}{2\pi^{1/2}w_c} \exp\left[-\frac{(v - \delta U_c)^2}{w_c^2}\right], w_c = \left(\frac{2\kappa_B T_c}{m_e}\right)^{1/2} \quad (3)$$

and the halo distribution component is given by

$$f_h^\kappa(v) = \frac{n_h}{\pi^{1/2}w_h} \frac{\Gamma(\kappa)}{\kappa^{1/2}\Gamma(\kappa - 1/2)} \left[1 + \frac{(v - \delta U_h)^2}{\kappa w_h^2}\right]^{-\kappa},$$

$$w_h = \left(\frac{2\kappa_B T_h}{m_e}\right)^{1/2}. \quad (4)$$

Both distribution function models has been superposed and fitted simultaneously to the reduced VDFs measurements. We also impose two physical constraints, i.e., the total density condition $n = n_c + n_h$ and the 0th parallel current condition $n_c \delta U_c + n_h \delta U_h = 0$.

[13] We initially fitted the resultant full 1-D reduced electron VDFs $f_e(v)$ data in a coordinate system relative to the local magnetic field B using a single Tsallis kappa-like distribution model as in equation (1) where the density, temperature, and drift velocity have been maintained fixed, as determined by the moment calculations, and the only unknown parameter, i.e., κ, was adjusted. The parameter κ dictates the degree of nonthermal effects since small κ values provide a measure of suprathermal tails, whereas for $\kappa \rightarrow \infty$ the VDF will approach a Maxwellian distribution. The fitting procedure used in the single kappa-like fit is based on the simplex method [*Daniels*, 1978], and the procedure involves the minimization of

$$\chi^2(\kappa) = \frac{1}{N - m} \sum_{i=0}^{N} \frac{\left[f_e^{\text{data}}(v) - f_e^{\text{model}}(v; \kappa)\right]^2}{\sigma_e^2} \quad (5)$$

with the model described in equation (1). The fitting procedure for the core-halo model was carried out minimizing a similar χ^2 function but using equations (3) and (4) and the nonlinear least squares Levenberg-Marquardt algorithm with unconstrained and constrained parameters by the moment estimates. To assess the quality of the fitting analysis, we show plots in Figure 6 of typical reduced VDFs data (i.e., asterisks) superposed with the model (i.e., solid line) to provide a visual goodness-of-fit measure of the minimization of the χ^2 function for VDFs of the three magnetic clouds events. From the fitting of the core-halo model we obtained six parameters corresponding to n_c, T_c, n_h, T_h, δU_r, and κ where δU_r is the core-halo relative drift correction (i.e., $\delta U_r = \delta U_h - \delta U_c$) also expressed as

$$\delta U_h = \frac{n_c}{n}\delta U_r, \quad \delta U_c = -\frac{n_h}{n_e}\delta U_r, \quad n = n_c + n_h. \quad (6)$$

[14] The procedure used was to obtain good initial guesses for the fit parameters of the Maxwellian core and the halo kappa from the data to initiate the iterative fitting scheme until convergence was obtained. This procedure was
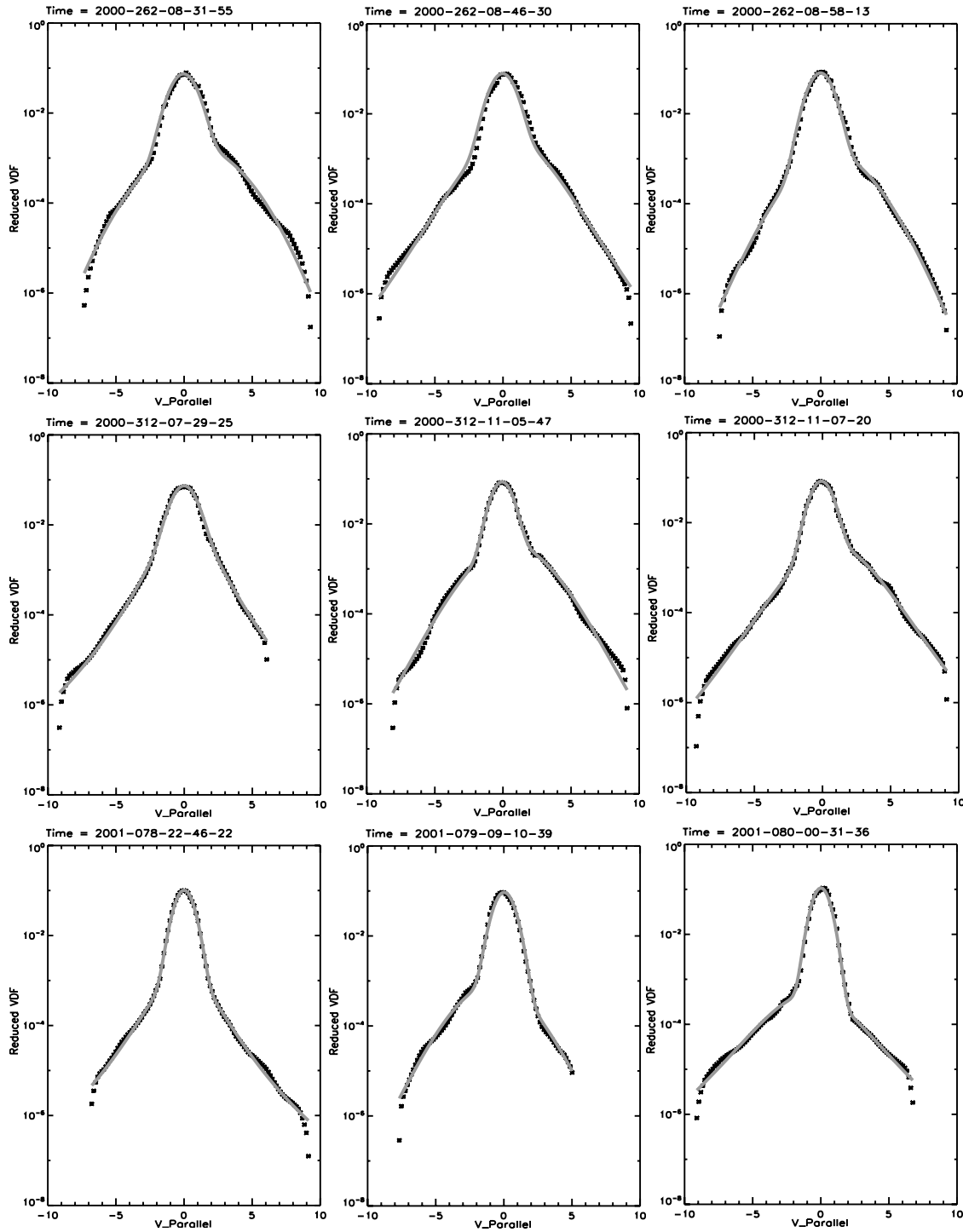
Figure 6. Sequence of typical reduced electron velocity distribution functions and the fitted model inside of the three magnetic cloud events.

carried out for each measured Wind SWE VEIS reduced distribution, which corresponds to about 6,500 measured VDFs per day. About 10% of the fitted results have been discarded because of no convergence, too many iterations required, or χ^2 values being too large. Some of the data were also discarded when the magnetic field elevation (inclination) angle was greater than ±54°, which is beyond the viewing angles of the VEIS detector, and therefore the

parallel information to reduce the distribution function is underestimated.

4. Statistical Results of the Model Fitting to the Observed Velocity Distribution Functions

[15] In this section we present the statistical results of the fitting analysis. Figure 7 shows histogram plots of the κ
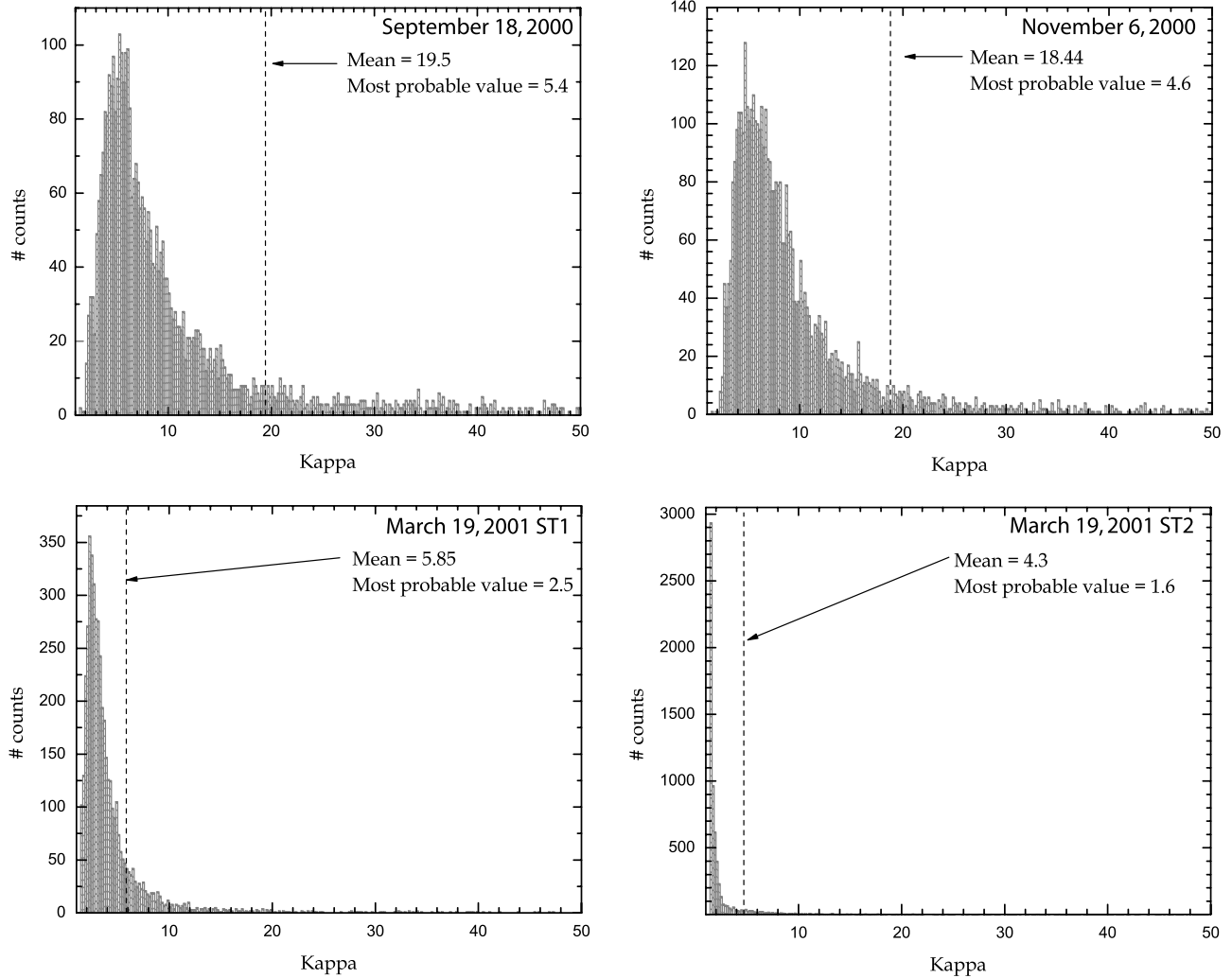
Figure 7. Histogram of the distribution of κ values inside the three magnetic cloud events showing the mean and the most probable κ values.

values inside the magnetic clouds for the three cloud events obtained from the fitting to a single Tsallis kappa-like distribution model. The histograms show the most probable κ values for the three magnetic clouds. The most probable κ values obtained inside the magnetic clouds ranged between 1.6 and 5.4, suggesting a significant suprathermal tails. However, similar statistical distributions are obtained (with $\kappa = 1.6$ to $\kappa = 6.1$) when the analysis is done outside the magnetic clouds as shown in Figure 8. The results of this statistical analysis indicate that there are no significant differences between the κ values inside and outside magnetic clouds or between cases where the temperature-density anticorrelation and no correlation were observed. Therefore we could not find any correlation which suggests that the single κ model of the electron VDF characterizes uniquely the magnetic clouds. Thus, although the electron VDFs inside seem to have a significant suprathermal component, such condition is not unique to magnetic clouds nor is it sensitive enough to provide a characteristic measure for the observed anticorrelation. Indeed, we have found as well as previous investigations [*Skoug et al.*, 2000a] similar anti-correlations outside magnetic clouds.

[16] The results of the core-halo analysis are summarized in Figures 9 and 10. Figure 9 shows a scatterplot of the core and halo temperature-density anticorrelation inside the magnetic cloud events. The result of this analysis clearly shows that the anticorrelation is seen primarily in the halo component and barely any correlation is seen in the core component. The polytrope index γ for the halo component is less than 1 in all cases, ranging in values from $0.55 \leq \gamma \leq 0.74$ and the most probable κ values ranging from 2.5 to 4. This implies that the temperature and density of the suprathermal components play a significant role in the temperature-density anticorrelation. A similar plot for the core and halo temperature-density anticorrelation outside (i.e., rear and front) the magnetic clouds is shown in Figure 10. The results again show that, in general, the halo component displays similar anticorrelation inside and outside the magnetic clouds. To ascertain the quality of the fits, we present in Figure 11 the estimated total density (core plus halo) versus the total moment density for the three cloud events investigated. Notice the linear relation between the estimated density ($n_{ec} + n_{eh}$) as a function of total moment density n_e indicating the good quality with
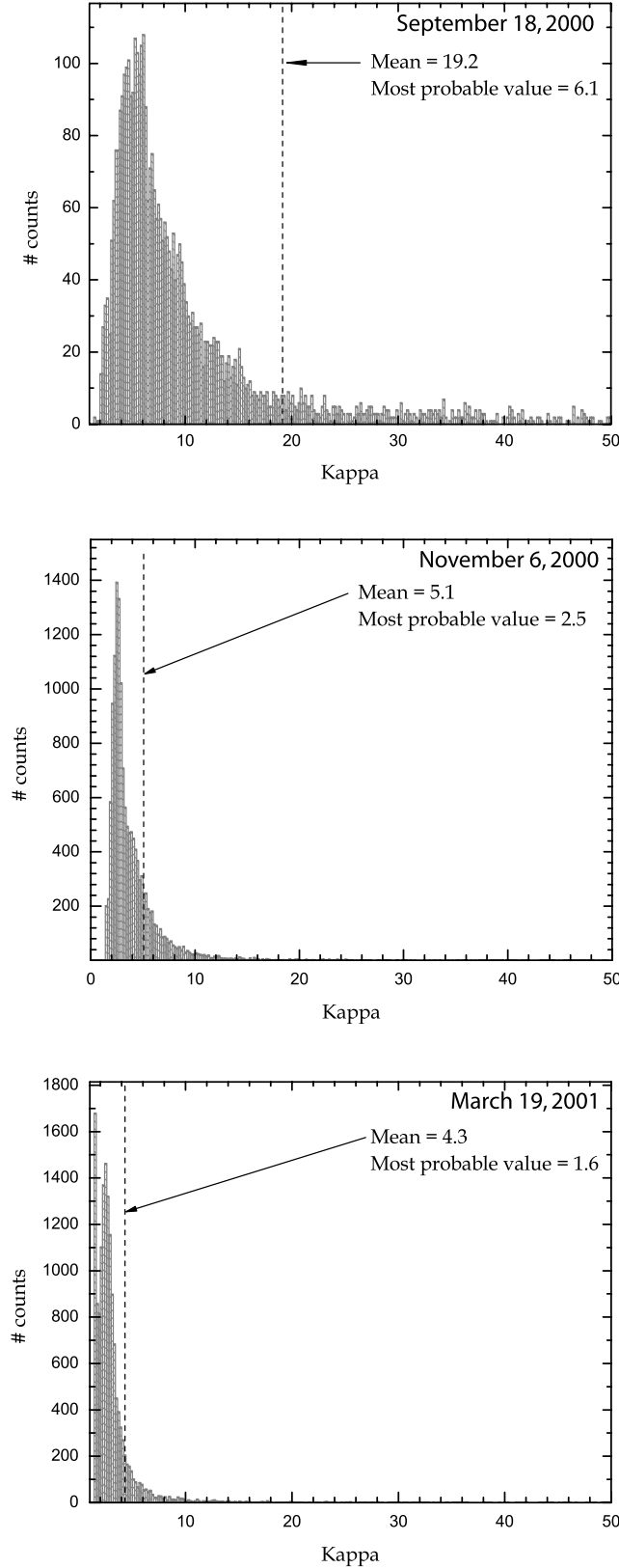
Figure 8. Histogram of the distribution of κ values outside the three magnetic cloud events showing the mean and the most probable κ values.

little dispersion of our calculations and the robustness of the constraints. Similarly, Figure 12 shows the linear correlation of the estimated effective electron temperature T_{eff} $((n_c T_c + n_h T_h)/(n_c + n_h))$ of the core and halo components versus the total moment temperature T_e, again showing little dispersion within the uncertainties of the data. The temperature correlation plot of the second structure (ST2) for the 19 March 2001 event in Figure 12 appears to have no linear correlation, when compared to the other events, because the observed range of moment temperatures is very limited with little dispersion. If the scale of moment temperatures T_e is changed to the range between 4×10^5 and 2×10^6, then the linear correlation will emerge, but the intercomparison with the other events will be lost. Nonetheless, the estimated effective temperatures T_{eff} were also limited with some dispersion (<2%), again suggesting consistency between the observed moment data and the estimated model results.

5. Polytrope Constant and the Kappa-Like Distribution Based Upon Entropy

[17] Beside the γ parameter the polytropic relation $P = \alpha n^\gamma$ also includes the parameter α that is related to the entropy of the system. Since we have assumed that these two parameters describe, at any time, the general behavior of the plasma inside the magnetic cloud, we therefore considered that whenever we observed a magnetic cloud, these two parameters will be assumed constant. Thus we cannot say what will be the evolution of the magnetic cloud beyond the observation point (i.e., 1 AU) nor we can describe the variation of these two parameters as a function of radial distance. For this we will have to follow in space and time (along the characteristics) the same magnetic cloud and measure the variations of these two parameters as a function of radial distance. Nonetheless, under this assumption we can find a theoretical relationship between the measure of suprathermal particles κ and the fluid polytropic relation $P_e = \alpha N_e^\gamma$ which can also be rewritten as

$$T^{1/(\gamma-1)}/n = T_0^{1/(\gamma-1)}/n_0 = \text{const} \qquad (7)$$

by invoking the physically relevant kinetic definition for the nonequilibrium entropy of a gas since the constant α is related to the entropy (i.e., the Boltzmann-Gibbs (BG) entropy [*Brey and Santos*, 1992])

$$S_{BG} \equiv -\kappa_B \iint f(v,r) \ln\{f(v,r)\} d^3v d^3r. \qquad (8)$$

[18] The parameters T_0 and n_0 in (7) are some reference temperature and density within the magnetic cloud. Here we follow a similar procedure as *Collier* [1995] but for a general gas described by an arbitrary pressure-density polytrope relation. We also use the normalized 3-D form of the Tsallis kappa-like distribution given by [see *Leubner*, 2004a]

$$f(v) = \frac{n}{\pi^{3/2} w^3} \frac{\Gamma(\kappa)}{\kappa^{3/2}\Gamma(\kappa - 3/2)} \left[1 + \frac{v^2}{\kappa w^2}\right]^{-\kappa}. \qquad (9)$$
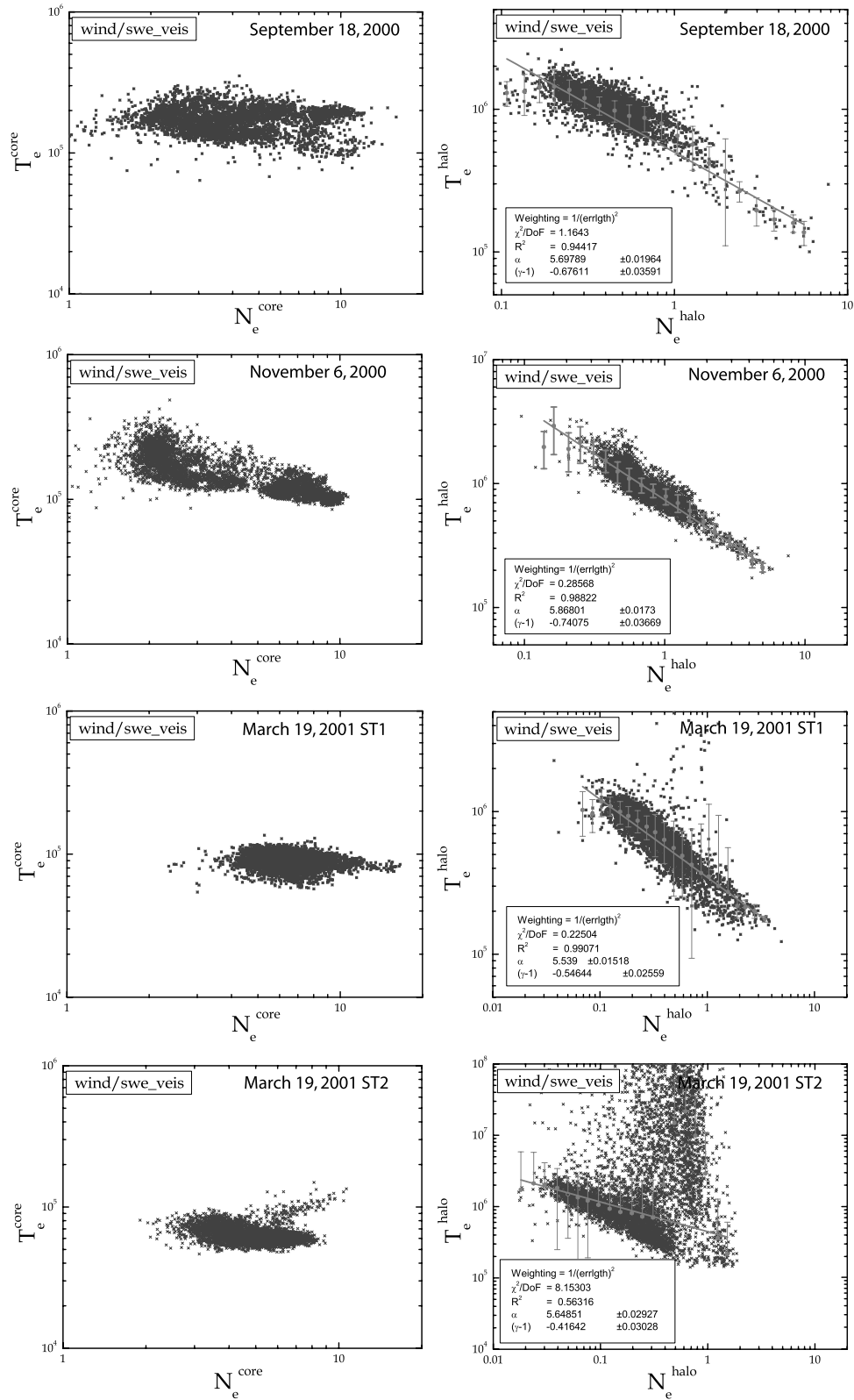
Figure 9. Scatterplots of the correlation of the core and halo electron temperature and density inside the magnetic clouds.
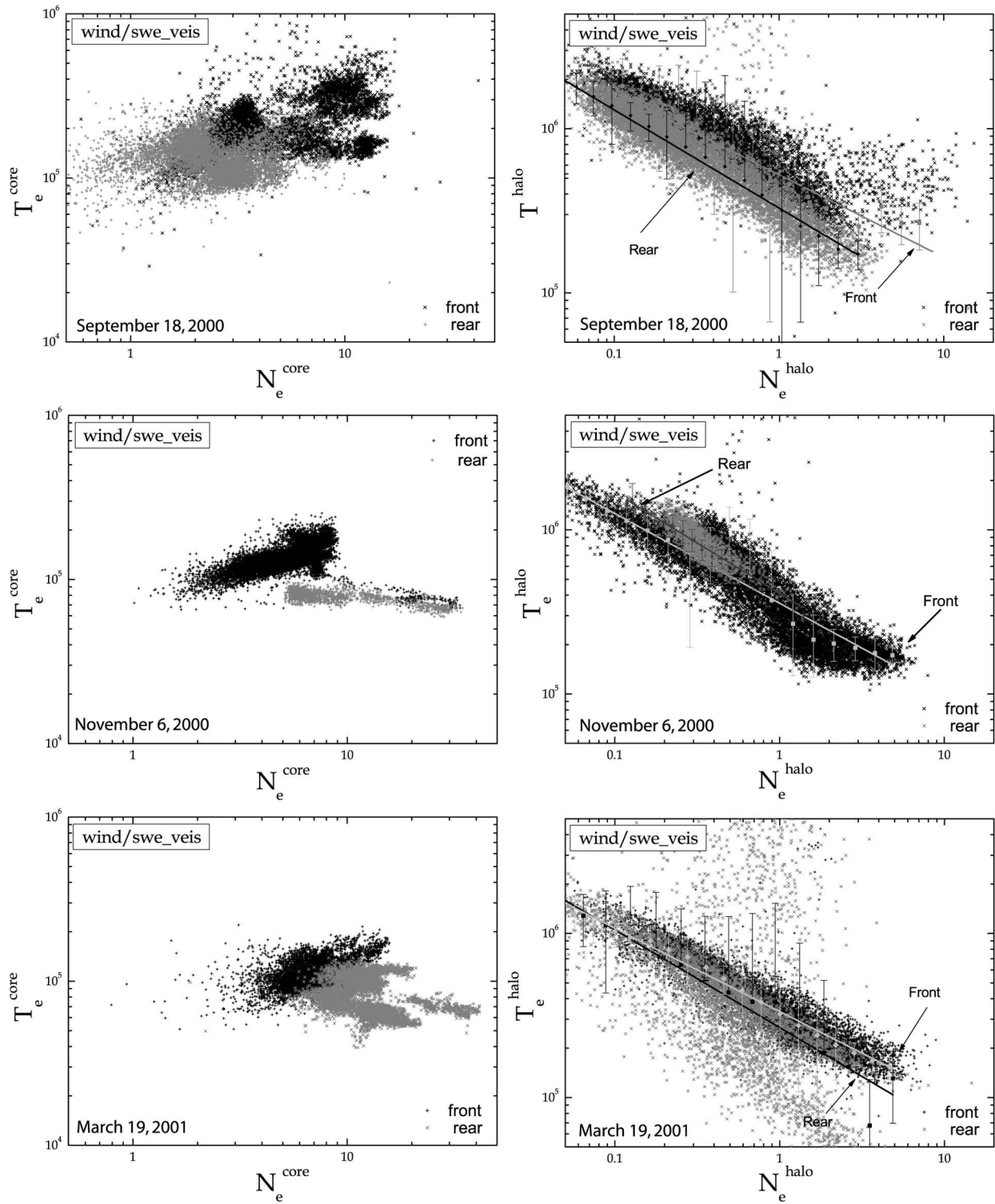
Figure 10. Scatterplots of the correlation of the core and halo electron temperature and density outside (front/rear) the magnetic clouds.
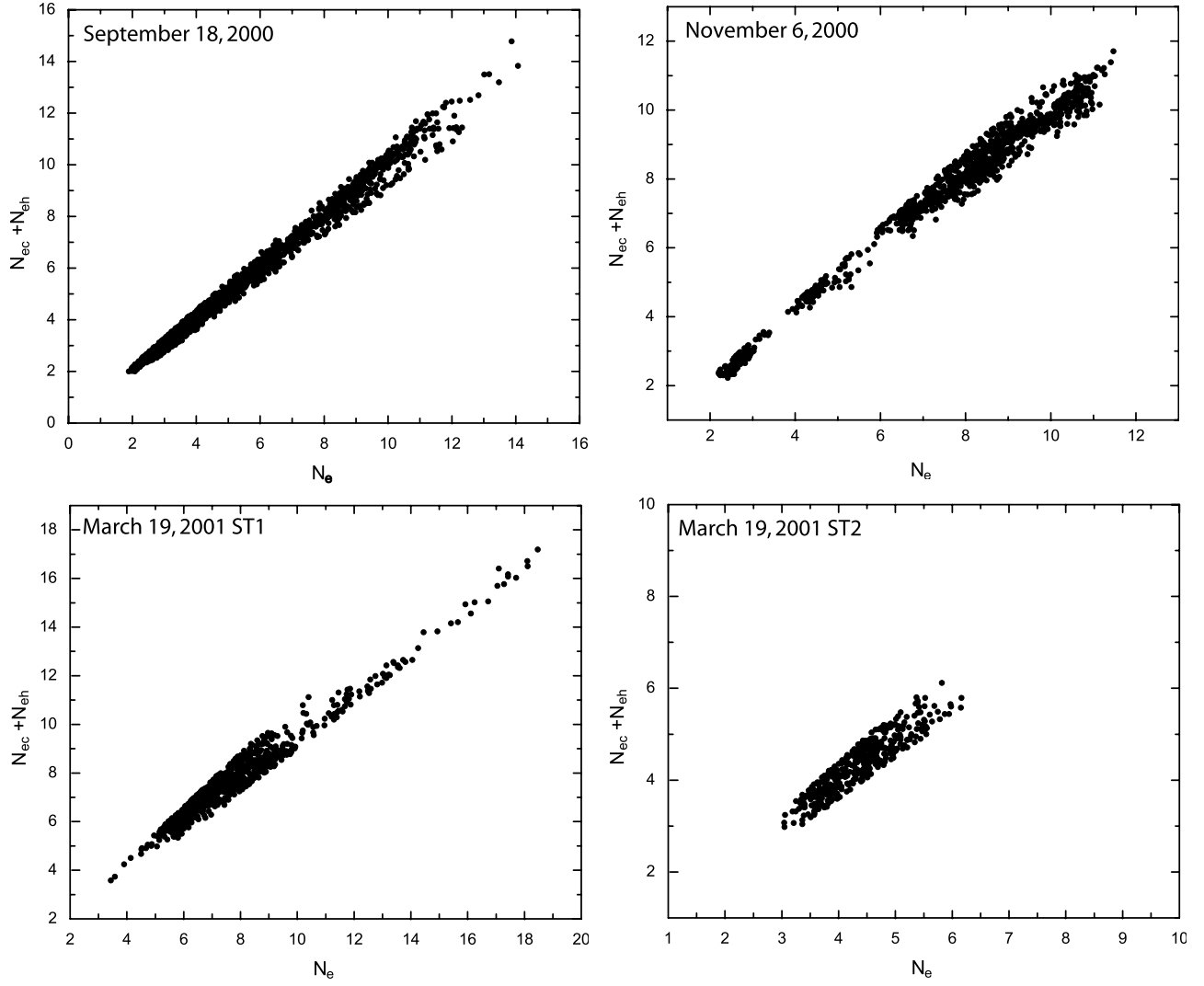
Figure 11. Scatterplot of the total electron (core plus halo) density estimated by the fits versus total moment electron density for the three magnetic cloud events.

When the kappa-like distribution model given in equation (9) (for an isotropic distribution function) is substituted into the BG entropy (8) and the integrals are performed, the resulting expression for the BG entropy per particle of a kappa-like distribution becomes

$$\frac{S_{BG}}{N\kappa_B} = \ln\left\{\frac{\pi^{3/2}T^{3/2}}{n}\frac{\kappa^{3/2}\Gamma(\kappa-3/2)}{\Gamma(\kappa)}\right\} + \kappa[\psi(\kappa) - \psi(\kappa-3/2)],$$

(10)

where ψ is the derivative of the gamma function (i.e., digamma function). Since the analogous fluid entropy is defined within a constant by $S_F/(N\kappa_B) = \ln(P/n^\gamma) = \ln(T^{1/(\gamma-1)}/n)$ then we obtain a relationship between the polytrope index γ and κ which is parametric on the temperature T/T_0

$$\gamma = \gamma_{BG}^\kappa = 1 + [\ln(\xi_{BG}(\kappa))/\ln(T/T_0) + 3/2]^{-1}$$

$$\xi_{BG}(\kappa) = \frac{\kappa^{3/2}\Gamma(\kappa-3/2)}{\Gamma(\kappa)}\exp(\kappa[\psi(\kappa) - \psi(\kappa-3/2)] - 3/2).$$

(11)

[19] At this point we recall that the kappa-like distribution function given in (9) is the resultant distribution for the maximization of the Tsallis entropy [*Tsallis*, 1988; *Tsallis and Brigatti*, 2004] in nonextensive statistical mechanics and not the resultant VDF of the maximization of the BG entropy (8). Thus it is necessary to perform a similar analysis using the Tsallis entropy function, since the kappa-like distribution in (9) is the proper solution of maximizing the Tsallis entropy within nonextensive statistical mechanics [*Tsallis*, 1988; *Tsallis and Brigatti*, 2004]. The Tsallis entropy per particle is originally defined by the q log and q exp operator definitions in nonextensive statistical mechanics as

$$\frac{S_T}{N\kappa_B} \equiv -\int f(v)\ln_q\{f(v)\}d^3v,$$

(12)

where the q log and q exp function definition are

$$\ln_q(x) = \frac{x^{1-q}-1}{1-q}, \quad \exp_q(x) = [1+(1-q)x]^{1/(1-q)}.$$
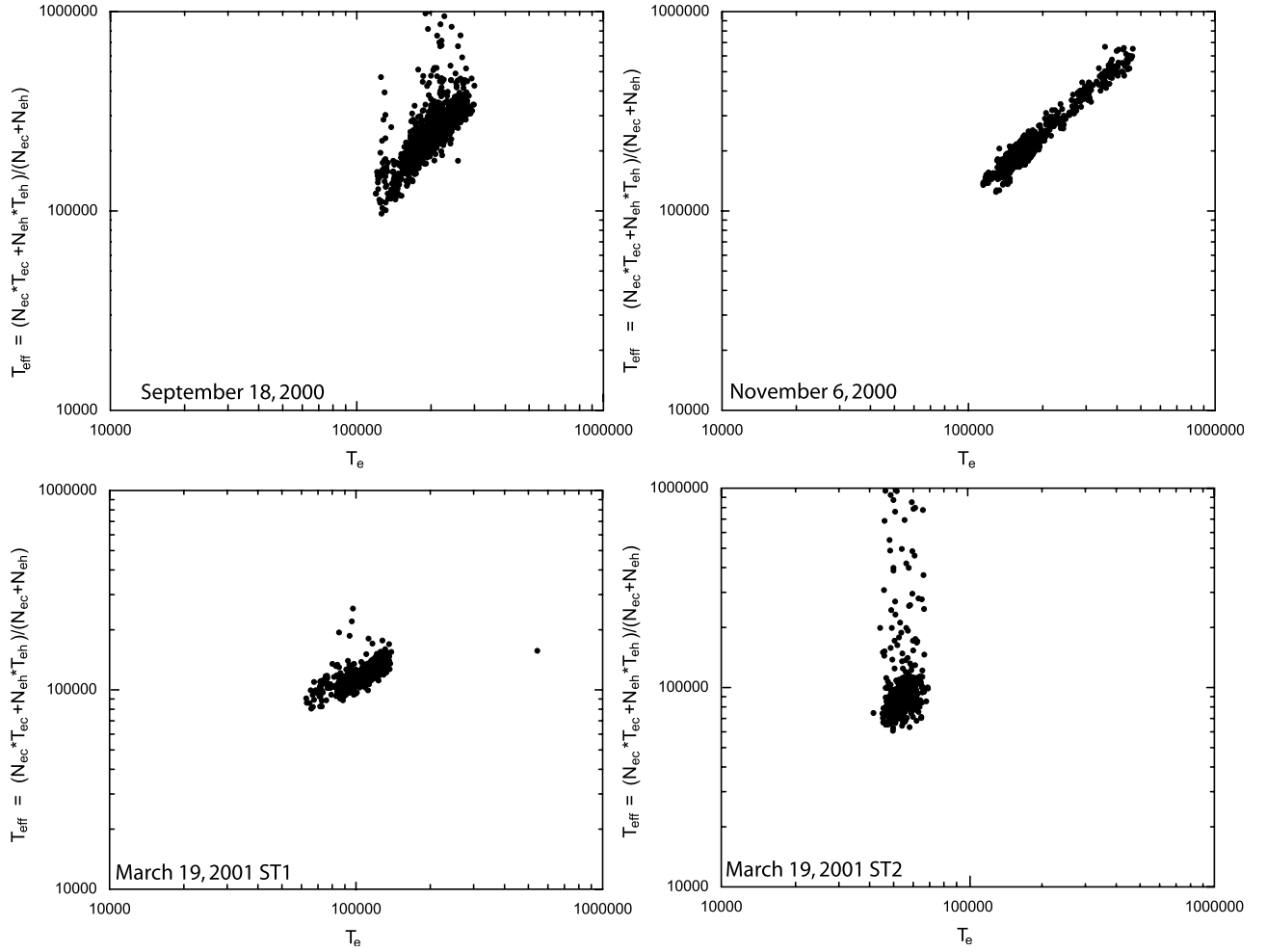
(13)

Figure 12. Scatterplot of the total effective electron (core plus halo) temperature estimated by the fits versus total moment electron temperature for the three magnetic cloud events.

[20] The connection between the Tsallis q distribution and the kappa-like distribution is given by $\kappa = 1/(q - 1)$ [see *Leubner*, 2004a]. Substitution of the kappa-like distribution (9) (for an isotropic 3-D model) into the Tsallis entropy (12) and carrying out the integrals the resulting expression for the Tsallis entropy per particle of a kappa-like distribution becomes

$$\frac{S_T}{N\kappa_B} \equiv \ln_\kappa \left\{ \frac{\pi^{3/2}T^{3/2}}{n} \frac{\kappa^{3/2}\Gamma(\kappa - 3/2)}{\Gamma(\kappa)} \left(\frac{\kappa}{\kappa - 3/2} \right)^\kappa \right\}, \quad (14)$$

and performing an analogous comparison with the fluid entropy, we obtain a relationship between the polytrope index γ and κ which is parametric on the temperature ratio T/T_0 and a constant given by

$$\gamma = \gamma_T^\kappa = 1 + [\ln(\xi_T(\kappa))/\ln(T/T_0) + 3/2]^{-1}$$

$$\xi_T(\kappa) = \frac{\kappa^{3/2}\Gamma(\kappa - 3/2)}{\Gamma(\kappa)} \left(\frac{\kappa}{\kappa - 3/2} \right)^\kappa \exp(-3/2). \quad (15)$$

[21] We have plotted the expressions for the polytrope index γ versus κ for both the Boltzmann-Gibbs and Tsallis

entropy analysis, parametric on T/T_0, to determine under what conditions the polytrope index γ becomes less than unity (i.e., $\gamma < 1$). The values for T and T_0 were chosen from the linear fit of the temperature-density anticorrelation within a magnetic cloud in Figure 4 by selecting their maximum and minimum values. The results of this calculation are shown in Figure 13 and they are only valid for constant entropy. The profile of the polytrope index γ versus κ under the Boltzmann-Gibbs and Tsallis entropies are very similar, indicating that only under very stringent conditions on the κ values does the polytrope index γ become less than unity (i.e., $\gamma < 1$). Note that κ has to be very close to 3/2 to get $\gamma < 1$. Furthermore, note that in the limit as κ approaches infinity the polytrope index γ approaches 5/3 (i.e., the adiabatic case) for both the BG and Tsallis entropies. Our theoretical results predicts that only for the most probable κ values of about $\kappa = 1.55$ will the polytrope index be $\gamma \approx 0.8 < 1$. Such condition in κ values are very stringent.

[22] *Scudder* [1992] has provided an expression (e.g., $\gamma = 1 - 1/(\kappa - 1/2)$) which relates the polytropic index to κ and is independent of temperature using the conventional form of the kappa distribution. Although we have been unable to
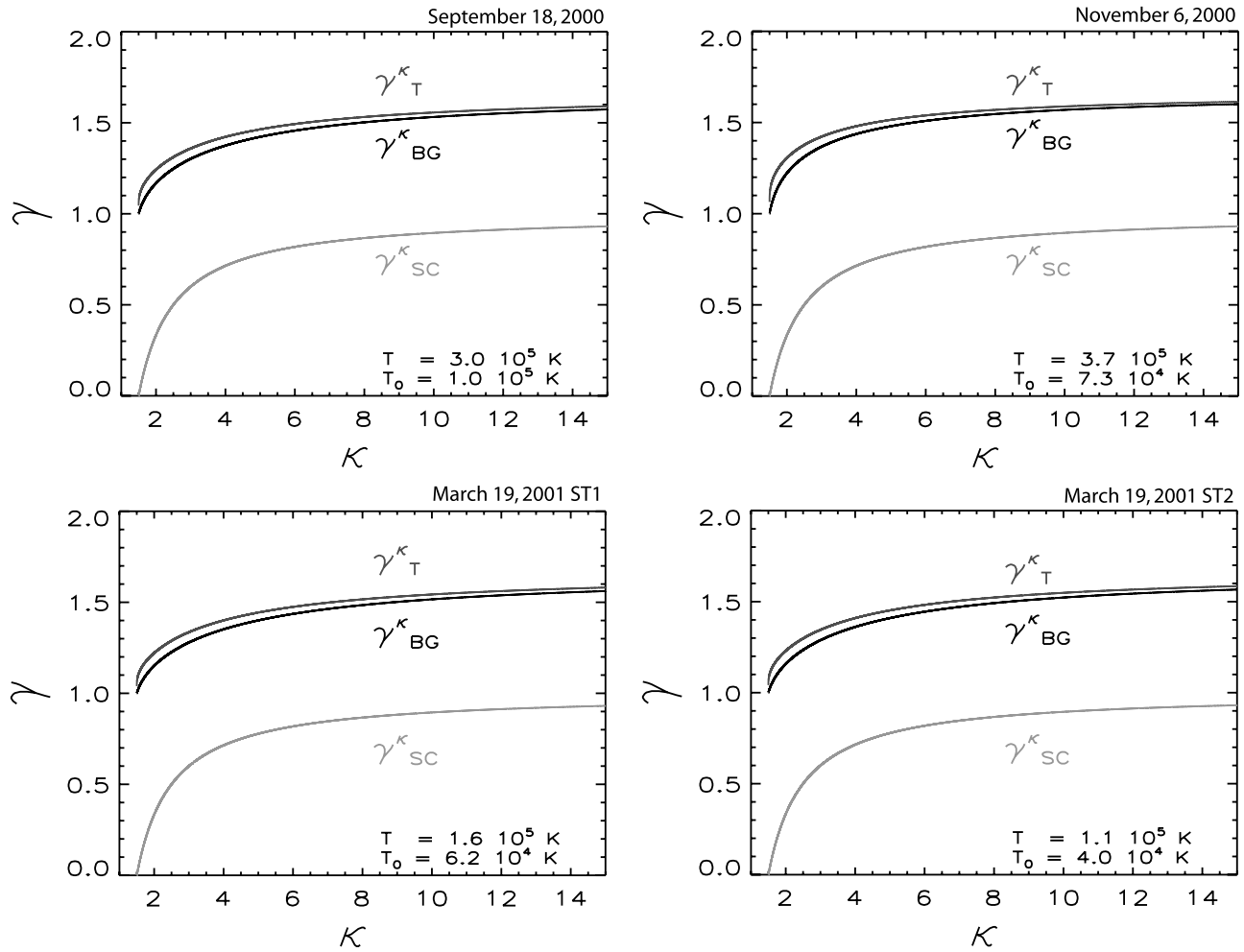
Figure 13. Plots of the polytrope coefficient γ versus κ values estimated from the Tsallis (γ_T) and Maxwell-Boltzmann (γ_{BG}) entropy relations and from *Scudder*'s [1992] (γ_{SC}) relation.

reproduce this relationship from first principles or to find out under what conditions such expression is valid, we have used it for comparison purposes. A plot of *Scudder* [1992] polytrope expression is also presented in Figure 13 for comparison. Note that as κ approaches infinity the polytrope index γ approaches 1 (i.e., the isothermal case). A further comparison with the Tsallis and Boltzmann-Gibbs polytrope relations shows that in the isothermal limit (i.e., where T approaches T_0) both polytropes expressions in equations (11) and (15) approaches 1 and becomes independent of κ and temperature. Using *Scudder*'s [1992] expression, we estimated the polytrope constant using the most probable values for κ as determined by our statistical analysis. The results using *Scudder*'s [1992] expression indicates that for the three magnetic clouds investigated in this study the values of γ ranged between 0.09 and 0.8.

6. Summary and Discussion

[23] The observations of the electron VDFs within magnetic clouds from the SWE VEIS and 3DP Berkeley instruments aboard Wind have provided an opportunity to examine the anticorrelation of the electron temperature

and density within clouds. Our analysis results showed that the electron temperature and densities are anticorrelated within magnetic clouds and that the slope of the anticorrelation γ is less than 1, consistent with previous investigations [*Osherovich et al.*, 1993, 1998; *Sittler and Burlaga*, 1998; *Skoug et al.*, 2000a, 2000b]. We have also showed that such anticorrelation is not unique to MCs and can also exist in regions outside the clouds in the solar wind, again consistent with previous results [*Skoug et al.*, 2000a, 2000b]. When we analyzed the VDFs outside the magnetic clouds, in the regions preceding and following the MCs, some showed no correlation at all, whereas others showed evidence of anticorrelation.

[24] The results of our modeling of the electron VDFs by a single 1-D kappa-like distribution showed that the association of the anticorrelation to the presence of suprathermal tails is at least ambiguous when such population is represented by a single kappa-like distribution. Although the statistical analysis shown demonstrates that the most probable κ values are small (from 1.6 to 5.4) within the MC, this is by no mean unique to MCs and similar statistical analysis outside MC show similar results. This result is similar and independent of whether one models the distribution function

using one or two dimensions in the velocity domain. The theoretical work of *Scudder* [1992] does predict that $\gamma < 1$ for a nonthermal plasma and also that the electrons behave isothermally in the limit as κ approaches infinity; however, suprathermal populations are not the only form of nonthermal effects in a plasma, since there are also temperature anisotropy effects, bidirectional heat flux, beams, etc. Thus this requires consideration when modeling the VDF.

[25] Our results also show a clear anticorrelation of the halo temperature with the halo density within magnetic clouds with typical halo component polytrope index $\gamma < 1$ in all cases, ranging from 0.55 to 0.74 and with κ values ranging from 2.5 to 4. However, almost no correlation was obtained when we compared the core temperature to core density. Similarly, we also observed a slight anticorrelation (not shown) between the halo-to-total (moment) density versus moment density. This clearly shows that the density-temperature anticorrelation observed in clouds is due to the relative enhancement of the halo abundance to the total density. It is clear that our results are consistent with the conclusion that the anticorrelation between the moment temperature and moment density is caused by changes in the halo population only and that the core population plays little or no role in such anticorrelation. Similarly, the core-halo analysis of the VDFs outside the magnetic clouds showed also evidence for a temperature-density anticorrelation in the halo component, suggesting that this relationship is not unique to magnetic clouds. Typical values of the estimated halo component polytrope index γ are generally less than 1, with $\gamma \sim 0.5$ in front and a smaller value $\gamma \sim 0.4$ in the rear. Our preliminary estimates seem to show that γ is usually smaller at the rear region than at the front of the magnetic cloud. Other interesting core-halo models have been proposed [*Leubner*, 2004b] which can be justified within Tsallis nonextensive statistical mechanics and may provide a better fit to the data. Such a model is being currently explored for a future publication. However, the results using such a model will not be significantly different from those obtained here with regards to the temperature-density anticorrelation. Furthermore, our main purpose was not to find which model provides a more accurate determination for a core-halo solar wind distribution but to provide a physical explanation within a kinetic description to the temperature-density anticorrelation.

[26] The theoretical question of why the anticorrelation is sensitive to the halo population only within magnetic clouds still needs to be addressed. We suggest that this may be due to the fact that the magnetic field lines within MC could be anchored to the Sun at both ends and the effect of the increased net heat fluxes (i.e., bidirectional fluxes), which are generated by the halo-counter-streaming electrons which are trapped and exposed to the hot corona of the Sun on both ends of the field lines, enhances the relative importance of halo electrons with respect to the core electrons. However, it is also reasonable to consider that *Scudder*'s [1992] solution shows that such anticorrelation can be explained for small κ values if the electrons are consistent with the isothermal limit. This aspect needs to be further investigated and leaves a possible explanation for the connection between the temperature-density anticorrelation and the presence of suprathermal particles, as measured by the small κ values. We would like to point out that, in general, the analysis must also include data from the strahl electron population, which has not yet been included on any model because of the difficulties of having a good dedicated strahl detector that can measure the angular width of this component as a function of energy with similar high time resolution as our Wind VEIS.

References

Brey, J. J., and A. Santos (1992), Nonequilibrium entropy of a gas, *Phys. Rev. A*, *45*, 8566.

Burlaga, L. F., E. Sittler, F. Mariani, and R. Schwenn (1981), Magnetic loop behind an interplanetary shock: Voyager, Helios and IMP 8 observations, *J. Geophys. Res.*, *86*, 6673.

Collier, M. R. (1995), The Adiabatic Transport of Superthermal Distributions Modelled by Kappa Functions, *Geophys. Res. Lett.*, *22*(19), 2673.

Daniels, R. W. (1978), *An Introduction to Numerical Methods and Optimization Techniques*, North-Holland, New York.

Dasso, S., C. J. Farrugia, F. T. Gratton, R. F. Lepping, K. W. Ogilvie, and R. J. Fitzenreiter (2001), Waves in the proton cyclotron frequency range in the CME observed by Wind on August 7–8, 1996: Theory and data, *Adv. Space Res.*, *28*(5), 747.

Dasso, S., F. T. Gratton, and C. J. Farrugia (2003), A parametric study of the influence of ion and electron properties on the excitation of electromagnetic ion cyclotron waves in coronal mass ejections, *J. Geophys. Res.*, *108*(A4), 1149, doi:10.1029/2002JA009558.

Dorelli, J. C., and J. D. Scudder (1999), Electron heat flow carried by kappa distributions in the solar corona, *Geophys. Res. Lett.*, *26*(23), 3537.

Fainberg, J., V. A. Osherovich, R. G. Stone, R. J. MacDowall, and A. Balogh (1996), Ulysses observations of electron and proton components in a magnetic cloud and related wave activity, *AIP Conf. Proc.*, *382*, 554.

Feldman, W. C., J. R. Asbridge, S. J. Bame, M. D. Montgomery, and S. P. Gary (1975), Solar wind electrons, *J. Geophys. Res.*, *80*, 4181.

Gosling, J. T. (1999), On the determination of electron polytrope indices within coronal mass ejections in the solar wind: Ulysses observations, *J. Geophys. Res.*, *104*, 19,851.

Gosling, J. T., D. N. Baker, S. J. Bame, W. C. Feldman, and R. D. Zwickl (1987), Bidirectional solar wind electron heat flux events, *J. Geophys. Res.*, *92*, 8519.

Hammond, C. M., J. L. Phillips, G. K. Crawford, and A. Balogh (1996), The relationship between electron density and temperature inside coronal mass ejections, *AIP Conf. Proc.*, *382*, 558.

Lepping, R. P., D. B. Berdichevsky, C.-C. Wu, A. Szabo, T. Narock, F. Mariani, A. J. Lazarus, and A. J. Quivers (2006), A summary of Wind magnetic clouds for the years 1995–2003: Model-fitted parameters, associated errors, and classifications, *Ann. Geophys.*, *24*(1), 215.

Leubner, M. P. (2004a), Fundamental issues on kappa-distributions in space plasmas and interplanetary proton distributions, *Phys. Plasmas*, *11*(4), 1308.

Leubner, M. P. (2004b), Core-halo distribution functions: A natural equilibrium state in generalized thermostatistics, *Astrophys. J.*, *604*, 469.

Lin, R. P., et al. (1995), A three-dimensional plasma and energetic particle investigation for the Wind spacecraft, in *The Global Geospace Mission*, ed. C. T. Russell, pp. 79–124, Kluwer Academic Publishers, Dordrecht, Netherlands.

Maksimovic, M., V. Pierrard, and P. Riley (1997), Ulysses Electron Distributions Fitted with Kappa Functions, *Geophys. Res. Lett.*, *24*(9), 1151.

Marsch, E. (2005), Kinetic physics of the solar corona and solar wind, *Living Rev. Sol. Phys.*, *3*, 1.

Nieves-Chinchilla, T., M. A. Hidalgo, and J. Sequeiros (2005), Magnetic clouds at 1 AU during the period 2000–2003, *Sol. Phy.*, *232*, 105.

Ogilvie, K. W., et al. (1995), A comprehensive plasma instrument for the Wind spacecraft, in *The Global Geospace Mission*, ed. C. T. Russell, pp. 55–77, Kluwer Academic Publishers, Dordrecht, Netherlands.

Olbert, S. (1968), Summary of experimental results from MIT detector on IMP-1, in *Physics of the Magnetosphere*, edited by R. L. Carovillano, J. F. McClay, and H. R. Radoski, pp. 641–659, Springer-Verlag, New York.

Osherovich, V. A., C. J. Farrugia, L. F. Burlaga, R. P. Lepping, J. Fainberg, and R. G. Stone (1993), Polytropic relationship in interplanetary magnetic clouds, *J. Geophys. Res.*, *98*, 15,331.

Osherovich, V. A., J. Fainberg, R. G. Stone, R. Fitzenreiter, and A. F. Viñas (1998), Measurements of Polytropic Index in the January 10–11, 1997 magnetic cloud observed by Wind, *Geophys. Res. Lett.*, *25*(15), 3003.

Pilipp, W. G., H. Miggenrieder, M. D. Montgomery, K.-H. Mühlhäuser, H. Rosenbauer, and R. Schwenn (1987), Unusual electron distribution functions in the solar wind derived from the helios plasma experiment: Double-strahl distributions and distributions with an extremely anisotropic core, *J. Geophys. Res.*, *92*(A2), 1093.

Russell, C. T., and A. A. Shinde (2005), On defining interplanetary coronal mass ejections from fluid parameters, *Sol. Phys.*, *229*, 323.

Scudder, J. D. (1992), On the cause of temperature change in inhomogeneous low density astrophysical plasmas, *Astrophys. J.*, *398*, 299.

Sittler, E. C., Jr., and L. F. Burlaga (1998), Electron temperatures within magnetic clouds between 2 and 4 AU: Voyager 2 observations, *J. Geophys. Res.*, *103*(A8), 17,447.

Skoug, R. M., W. C. Feldman, J. T. Gosling, D. J. McComas, and C. W. Smith (2000a), Solar wind electron characteristics inside and outside coronal mass ejections, *J. Geophys. Res.*, *105*(A10), 23,069.

Skoug, R. M., W. C. Feldman, J. T. Gosling, D. J. McComas, D. B. Reisenfeld, C. W. Smith, R. P. Lepping, and A. Balogh (2000b), Radial variation of solar wind electrons inside a magnetic cloud observed at 1 and 5 AU, *J. Geophys. Res.*, *105*(A12), 27,269.

Tsallis, C. (1988), Possible generalization of Boltzmann-Gibbs statistics, *J. Stat. Phys.*, *52*, 479.

Tsallis, C., and E. Brigatti (2004), Nonextensive statistical mechanics: A brief introduction, *Continuum Mech. Thermodyn.*, *16*, 223.

Vasyliunas, V. M. (1968), A survey of low-energy electrons in the evening sector of the magnetosphere with OGO 1 and OGO 3, *J. Geophys. Res.*, *73*, 2839.

―――――――――――――

T. Nieves-Chinchilla and A. F. Viñas, Geospace Physics Laboratory, NASA Goddard Space Flight Center, Mail Code 673, Greenbelt, MD 20771, USA. (adolfo.figueroa-vinas.1@gsfc.nasa.gov)